Available online at www.sciencedirect.com
ScienceDirect
Journal of Solid State Chemistry 180 (2007) 3560–3570
JOURNAL OF SOLID STATE CHEMISTRY
www.elsevier.com/locate/jssc

Synthesis, crystal structures, phase transition characterization and thermal decomposition of a new dabcodiium hexaaquairon(II) bis(sulfate): $(C_6H_{14}N_2)[Fe(H_2O)_6](SO_4)_2$

Samia Yahyaoui[a], Walid Rekik[a,b], Houcine Naïli[a], Tahar Mhiri[a], Thierry Bataille[b,*]

[a]*Laboratoire de l'Etat Solide, Département de Chimie, Faculté des Sciences de Sfax, BP 802, 3018 Sfax, Tunisia*
[b]*Laboratoire Sciences Chimiques de Rennes (CNRS, UMR 6226), Groupe Matériaux Inorganiques: Chimie Douce et Réactivité, Université de Rennes 1, Avenue du Général Leclerc, 35042 Rennes Cedex, France*

Received 29 June 2007; received in revised form 12 October 2007; accepted 16 October 2007
Available online 23 October 2007

Abstract

The crystal structures of 1,4-diazabicyclo[2.2.2]octane (dabco)-templated iron sulfate, $(C_6H_{14}N_2)[Fe(H_2O)_6](SO_4)_2$, were determined at room temperature and at −173 °C from single-crystal X-ray diffraction. At 20 °C, it crystallises in the monoclinic symmetry, centrosymmetric space group $P2_1/n$, $Z=2$, $a=7.964(5)$, $b=9.100(5)$, $c=12.065(5)$ Å, $\beta=95.426(5)^\circ$ and $V=870.5(8)$ Å^3. The structure consists of $[Fe(H_2O)_6]^{2+}$ and disordered $(C_6H_{14}N_2)^{2+}$ cations and $(SO_4)^{2-}$ anions connected together by an extensive three-dimensional H-bond network. The title compound undergoes a reversible phase transition of the first-order at −2.3 °C, characterized by DSC, dielectric measurement and optical observations, that suggests a relaxor–ferroelectric behavior. Below the transition temperature, the compound crystallizes in the monoclinic system, non-centrosymmetric space group *Cc*, with eight times the volume of the ambient phase: $a=15.883(3)$, $b=36.409(7)$, $c=13.747(3)$ Å, $\beta=120.2304(8)^\circ$, $Z=16$ and $V=6868.7(2)$ Å^3. The organic moiety is then fully ordered within a supramolecular structure. Thermodiffractometry and thermogravimetric analyses indicate that its decomposition proceeds through three stages giving rise to the iron oxide.

Keywords: Chemical preparation; Crystal structure; Phase transition; Dielectric properties; Optical observation; Thermal decomposition

1. Introduction

The chemistry of organically templated metal sulfates has regained great interest because of the wide variety of crystal structures obtained with numerous amines, with 0D [1–5], 1D [6,7], 2D [8–11] and 3D [8,12–14] characters. In addition, ferroelastic and ferroelectric properties have been found in some double sulfates of trivalent metal with monovalent aliphatic ammonium cations [15–19]. Using this literature, we challenge to prepare new sulfate materials exhibiting ferroelectric or ferroelastic properties and open-framework structures. Many double sulfates combining transition metal and amine are of supramolecular fashion when prepared at room temperature [1–5,20–22]. By analogy with trivalent metal sulfates showing a para-ferroelectric transition upon cooling, it was expected that such divalent metal sulfates would exhibit this feature. The use of non-centrosymmetric amine groups, instead of alkylamines, may help crystallize disordered phases at room temperature. Cation ordering at low temperature would thus provide acentric structures, that is the basic condition to have ferroelectricity.

For this purpose, we have synthesized a new compound using 1,4-diazabicyclo[2.2.2]octane (hereafter referred to as dabco) as a template and iron(II) as transition metal. Here we report the chemical preparation, the crystal structure determination of the high-temperature and low-temperature phases (further referred to as HT- and LT-phases) as well as the phase transition characterized by differential scanning calorimetry (DSC), dielectric measurements, optical observations and the thermal behavior of the title compound.

*Corresponding author.
E-mail address: thierry.bataille@univ-rennes1.fr (T. Bataille).

0022-4596/$ - see front matter © 2007 Elsevier Inc. All rights reserved.
doi:10.1016/j.jssc.2007.10.019

2. Experimental

2.1. Material preparation

Single crystals of the title compound were grown by slow evaporation at room temperature of an aqueous solution of iron(II) sulfate heptahydrate, $FeSO_4 \cdot 7H_2O$, dabco, $C_6H_{12}N_2$, and concentrated sulfuric acid (H_2SO_4), in an equimolar ratio of 1 mmol in 10 mL of water. Crystal shape is an irregular prism with the characteristic green color of octahedrally coordinated Fe^{II}.

2.2. Single-crystal data collection and structure determination

The same suitable single crystal was used for collecting X-ray diffraction data at 20 and −173 °C. It was glued to a glass fiber mounted on a 4-circle Nonius KappaCCD area-detector diffractometer. Intensity data sets were collected using MoKα ($\lambda = 0.71073$ Å) through the program COLLECT [23]. Correction for Lorentz-polarization effect, peak integration and background determination was carried out with the program DENZO [24]. Frame scaling and unit cell parameters refinement were performed with the program SCALEPACK [24]. Analytical absorption corrections were performed by modeling the crystal faces [25] and empirical ones using Xabs2 [26] for the HT- and the LT-phases, respectively. Crystallographic data at 20 and −173 °C are listed in Table 1.

Both structures were solved in the monoclinic symmetry, in the centrosymmetric space group $P2_1/n$ at 20 °C and the non-centrosymmetric one Cc at −173 °C. Iron and sulfur atoms were located using the direct methods with program SHELXS-97 [27]. The oxygen atoms and the organic moieties were found from successive difference Fourier calculations using SHELXL-97 [28]. In the room temperature phase, all H atoms were located by difference Fourier syntheses after several cycles of least-squares refinements. H–O and H–H distances, within water molecules, were restrained to 0.85(2) and 1.39(2) Å, respectively. C–H and H–H distances within the disordered organic moiety were also constrained to 0.97(2) and 1.58(4) Å, respectively, so that the H–C–H angles fitted the ideal values of tetrahedral angle. In the low-temperature phase, the aqua H atoms were located in a difference Fourier map and their positions and isotropic displacement parameters were refined. H–O and H–H distances, within water molecules, were restrained to 0.96(1) and 1.50(1) Å, respectively, so that the H–O–H angles fitted the theoretical value of 105.4°. H atoms bonded to C and N atoms were positioned geometrically (the C–H and N–H bonds were fixed at 0.97 and 0.91 Å, respectively) and allowed to ride on their parent atoms. Selected bond distances and angles calculated from the final atomic coordinates are given in Table 2.

Table 1
Crystallographic data for $(C_6H_{14}N_2)[Fe(H_2O)_6](SO_4)_2$

Empirical formula	$C_6\ H_{26}\ Fe\ N_2\ O_{14}\ S_2$	$C_6\ H_{26}\ Fe\ N_2\ O_{14}\ S_2$
Formula weight	470.26	470.26
Temperature (°C)	20(2)	−173(2)
Crystal system	Monoclinic	Monoclinic
Space group	$P2_1/n$	Cc
a(Å)	7.964(5)	15.8833(3)
b(Å)	9.100(5)	36.4093(7)
c(Å)	12.065(5)	13.7469(3)
ß (°)	95.426(5)	120.2304(8)
V(Å^3)	870.5(8)	6868.7(2)
Z	2	16
ρ_{cal} (g cm^{-1})	1.794	1.814
Crystal size (mm^3)	0.324 × 0.178 × 0.122	0.324 × 0.178 × 0.122
Habit-color	Prism-green	Prism-green
λ (MoKα) (Å)	0.71073	0.71073
μ(mm^{-1})	1.179	1.193
θ range (°)	2.81–27.47	2.97–27.49
Index ranges	$-10 \leqslant h \leqslant 10$ $-11 \leqslant k \leqslant 11$ $-15 \leqslant l \leqslant 15$	$-20 \leqslant h \leqslant 20$ $-0 \leqslant k \leqslant 47$ $-17 \leqslant l \leqslant 17$
Unique data	1975	15118
Observed data [$I > 2\sigma(I)$]	1748	11055
F(000)	492	3936
Extinction coefficient	0.016(5)	0.00016(4)
Refinement method	Full matrix least-squares on $\|F^2\|$	Full matrix least-squares on $\|F^2\|$
R_1	0.0365	0.0500
WR_2	0.0948	0.1088
GooF	1.077	1.208
No. parameters	204	1044
Transmission factors	0.77891 and 0.88413	0.7393 and 0.9096
Largest difference map hole and peak (eÅ^{-3})	−0.475 and 0.773	−0.948 and 1.033

2.3. Thermal behavior

The differential scanning calorimetry analysis was performed with a SETARAM DSC131 instrument for temperatures ranging from −50 to 50 °C at a rate of 5 °C min^{-1}. A polycrystalline sample of 22.08 mg was placed in a hermetic aluminum cell into a nitrogen atmosphere.

The measurements of the complex electric permittivity, ε*, were performed with an impedance analyzer Hewlett-Packard 4192 A LF in the frequency range 100 Hz –13 MHz. Crystals of the title compound were crushed and pressed to dense and translucent pellets (8 mm in diameter; 0.75 mm in thickness) at a pressure of 200 MPa. Both planar faces of these pellets were coated with silver paint and the pellets were then sandwiched between metal electrodes, which were also coated with silver paint. The measurements were carried out in vacuum between −235 and 47 °C.

A thermogravimetric (TG) measurement was performed with a Rigaku Thermoflex instrument under flowing air, with a heating rate of 15 °C h^{-1} from ambient temperature

Table 2
Selected bond distances (Å) and angles (°)

$(C_6H_{14}N_2)[Fe(H_2O)_6](SO_4)_2$ (20 °C)					
Octahedron around Fe					
Fe–OW1	2.109(2)	OW1–Fe–OW2	92.82(8)	OW1–Fe–OW3^{I}	92.71(7)
Fe–OW2	2.115(2)	OW1–Fe–OW2^{I}	87.18(8)	OW2–Fe–OW3	89.22(9)
Fe–OW3	2.123(2)	OW1–Fe–OW3	87.29(7)	OW2–Fe–OW3^{I}	90.78(9)
Within the organic moiety					
N–C1	1.432(6)	C1–N–C2	115.1(5)		
N–C2	1.435(6)	C1–N–C5	109.6(5)		
N–C5	1.535(5)	C2–N–C5	107.5(5)		
N–C3	1.452(6)	C3–N–C4	112.7(5)		
N–C4	1.461(6)	C3–N–C6	109.3(4)		
N–C6	1.545(5)	C4–N–C6	106.1(4)		
C1–C3^{II}	1.516(9)	N–C1–C3^{II}	109.0(4)		
C2–C4^{II}	1.508(8)	N–C2–C4^{II}	108.2(4)		
C5–C6^{II}	1.531(7)	N–C5–C6^{II}	107.4(4)		
Symmetry codes: $^{I}-x+1, -y+1, -z+1$; $^{II}-x+1, -y+1, -z+2$.					
$(C_6H_{14}N_2)[Fe(H_2O)_6](SO_4)_2$ (−173 °C)					
Octahedron Fe1$(H_2O)_6$					
Fe1–OW11	2.101(4)	OW11–Fe1–OW12	93.1(2)	OW12–Fe1–OW15	86.8(2)
Fe1–OW12	2.106(5)	OW11–Fe1–OW13	177.7(2)	OW12–Fe1–OW16	93.6(2)
Fe1–OW13	2.117(4)	OW11–Fe1–OW14	86.9(2)	OW13–Fe1–OW14	94.5(2)
Fe1–OW14	2.118(4)	OW11–Fe1–OW15	90.5(2)	OW13–Fe1–OW15	91.4(2)
Fe1–OW15	2.130(4)	OW11–Fe1–OW16	90.3(2)	OW13–Fe1–OW16	87.8(2)
Fe1–OW16	2.145(4)	OW12–Fe1–OW13	85.7(2)	OW14–Fe1–OW15	91.7(2)
		OW12–Fe1–OW14	178.5(2)	OW14–Fe1–OW16	87.9(2)
				OW15–Fe1–OW16	179.1(2)
Octahedron Fe2$(H_2O)_6$					
Fe2–OW21	2.110(4)	OW21–Fe2–OW22	93.2(2)	OW22–Fe2–OW25	177.8(2)
Fe2–OW22	2.110(4)	OW21–Fe2–OW23	91.2(2)	OW22–Fe2–OW26	87.6(2)
Fe2–OW23	2.117(4)	OW21–Fe2–OW24	178.2(2)	OW23–Fe2–OW24	88.5(2)
Fe2–OW24	2.122(5)	OW21–Fe2–OW25	86.1(2)	OW23–Fe2–OW25	91.0(2)
Fe2–OW25	2.122(4)	OW21–Fe2–OW26	86.8(2)	OW23–Fe2–OW26	177.5(2)
Fe2–OW26	2.138(4)	OW22–Fe2–OW23	91.1(2)	OW24–Fe2–OW25	92.1(2)
		OW22–Fe2–OW24	88.6(2)	OW24–Fe2–OW26	93.6(2)
				OW25–Fe2–OW26	90.2(2)
Octahedron Fe3$(H_2O)_6$					
Fe3–OW31	2.117(4)	OW31–Fe3–OW32	89.7(2)	OW32–Fe3–OW35	92.7(2)
Fe3–OW32	2.122(4)	OW31–Fe3–OW33	179.1(2)	OW32–Fe3–OW36	179.1(2)
Fe3–OW33	2.122(4)	OW31–Fe3–OW34	91.0(2)	OW33–Fe3–OW34	89.8(2)
Fe3–OW34	2.124(5)	OW31–Fe3–OW35	88.2(2)	OW33–Fe3–OW35	91.0(2)
Fe3–OW35	2.126(4)	OW31–Fe3–OW36	90.2(2)	OW33–Fe3–OW36	90.1(2)
Fe3–OW36	2.145(4)	OW32–Fe3–OW33	90.1(2)	OW34–Fe3–OW35	179.3(2)
		OW32–Fe3–OW34	87.3(2)	OW34–Fe3–OW36	93.5(2)
				OW35–Fe3–OW36	86.4(2)
Octahedron Fe4$(H_2O)_6$					
Fe4–OW41	2.093(4)	OW41–Fe4–OW42	179.9(3)	OW42–Fe4–OW45	85.8(2)
Fe4–OW42	2.096(5)	OW41–Fe4–OW43	92.7(2)	OW42–Fe4–OW46	94.6(2)
Fe4–OW43	2.098(4)	OW41–Fe4–OW44	86.3(2)	OW43–Fe4–OW44	178.9(2)
Fe4–OW44	2.106(4)	OW41–Fe4–OW45	94.3(2)	OW43–Fe4–OW45	91.8(2)
Fe4–OW45	2.159(4)	OW41–Fe4–OW46	85.4(2)	OW43–Fe4–OW46	89.3(2)
Fe4–OW46	2.169(4)	OW42–Fe4–OW43	87.2(2)	OW44–Fe4–OW45	88.1(2)
		OW42–Fe4–OW44	93.9(2)	OW44–Fe4–OW46	90.8(2)
				OW45–Fe4–OW46	178.8(2)
Within dabco1					
N1–C1	1.491(7)	C1–N1–C2	109.3(5)	N1–C1–C6	108.8(4)
N1–C2	1.492(7)	C1–N1–C3	109.9(5)	N1–C2–C5	108.2(4)
N1–C3	1.494(7)	C2–N1–C3	110.6(5)	N1–C3–C4	108.3(4)
N2–C4	1.482(7)	C4–N2–C5	110.8(5)	N2–C4–C3	108.8(4)
N2–C5	1.495(7)	C4–N2–C6	109.4(5)	N2–C5–C2	108.6(4)

Table 2 (*continued*)

N2–C6	1.504(7)	C5–N2–C6	109.3(5)	N2–C6–C1	108.0(4)
C1–C6	1.527(7)				
C2–C5	1.527(7)				
C3–C4	1.521(6)				
Within dabco2					
N3–C7	1.482(8)	C7–N3–C8	109.3(5)	N3–C7–C10	107.8(5)
N3–C8	1.496(7)	C7–N3–C9	109.8(5)	N3–C8–C12	108.5(4)
N3–C9	1.502(7)	C8–N3–C9	110.7(5)	N3–C9–C11	107.5(4)
N4–C10	1.469(8)	C10–N4–C11	111.0(5)	N4–C10–C7	108.8(4)
N4–C11	1.491(7)	C10–N4–C12	109.8(5)	N4–C11–C9	108.3(4)
N4–C12	1.502(7)	C11–N4–C12	109.5(5)	N4–C12–C8	107.2(4)
C7–C10	1.528(7)				
C8–C12	1.537(6)				
C9–C11	1.525(7)				
Within dabco3					
N5–C13	1.482(7)	C13–N5–C14	109.7(5)	N5–C13–C17	108.7(4)
N5–C14	1.488(7)	C13–N5–C15	109.5(5)	N5–C14–C18	109.0(4)
N5–C15	1.490(7)	C14–N5–C15	110.6(5)	N5–C15–C16	108.4(4)
N6–C16	1.481(7)	C16–N6–C17	110.2(5)	N6–C16–C15	109.4(4)
N6–C17	1.483(7)	C16–N6–C18	110.4(5)	N6–C17–C13	109.4(4)
N6–C18	1.496(7)	C17–N6–C18	109.3(5)	N6–C18–C14	107.2(4)
C13–C17	1.508(7)				
C14–C18	1.546(6)				
C15–C16	1.507(7)				
Within dabco4					
N7–C19	1.472(7)	C19–N7–C20	110.0(5)	N7–C19–C23	109.0(4)
N7–C20	1.479(7)	C19–N7–C21	110.6(5)	N7–C20–C22	109.6(4)
N7–C21	1.491(7)	C20–N7–C21	109.7(5)	N7–C21–C24	108.5(4)
N8–C22	1.483(7)	C22–N8–C23	110.4(4)	N8–C22–C20	108.4(4)
N8–C23	1.493(6)	C22–N8–C24	109.0(4)	N8–C23–C19	109.5(4)
N8–C24	1.503(6)	C23–N8–C24	109.3(4)	N8–C24–C21	109.2(4)
C19–C23	1.506(6)				
C20–C22	1.519(6)				
C21–C24	1.516(5)				

to 900 °C. The powdered sample, 117.16 mg, was spread evenly in a large platinum crucible to avoid mass effects.

Temperature-dependent X-ray diffraction (TDXD) was performed with a D5005 powder diffractometer (Bruker AXS) using Cu$K\alpha$ radiation [$\lambda(K\alpha_1) = 1.5406$ Å, $\lambda(K\alpha_2) = 1.5444$ Å] selected with a diffracted-beam graphite monochromator, and equipped with an Anton Paar HTK1200 high-temperature oven camera. The thermal decomposition of the compound was carried out in air, with a heating rate of 14.4 °C h^{-1} from ambient to 870 °C. Temperature calibration was carried out with standard materials in the involved temperature range.

3. Results

3.1. Crystal structures

3.1.1. Room temperature structure (at 20 °C)

The crystal structure of $(C_6H_{14}N_2)[Fe(H_2O)_6](SO_4)_2$ at room temperature clearly shows that the interactions are dominated by hydrogen bonds. Indeed, the structure consists of isolated transition metals, Fe(II), octahedrally coordinated by six water molecules, sulfate tetrahedra and disordered dabcodiium cations linked together by a hydrogen bond network only (Fig. 1).

In the HT-phase structure, the iron atom occupies a special position on the inversion center, so that it is coordinated by six water oxygen atoms from which three are crystallographically independent. The octahedron thus formed is slightly distorted according to the Fe–OW distances and the *cis*-OW–Fe–OW angles (Table 2). The $FeOW_6$ octahedra are isolated from one to each other with a shortest distance Fe–Fe = 7.964 Å. This metal–metal distance is longer than those found in the related Ni and Cu compounds [3,4], in which the shortest Ni–Ni and Cu–Cu distances are equal to 7.000 and 6.953 Å, respectively. The gravity center of the organic cations also coincides with the inversion center of the unit cell. However, its internal symmetry, D_{3h}, does not allow any inversion center, so that the diamine adopts two possible orientations. The C atoms are distributed between two positions related by the center of symmetry, with a site occupancy factor equal to 0.5. Within the organic moiety, the N–C distances and the C–N–C angles range from 1.432(6) to 1.545(5) Å and from 106.1(4) to 115.1(5)°, respectively. These values, in agreement with those found

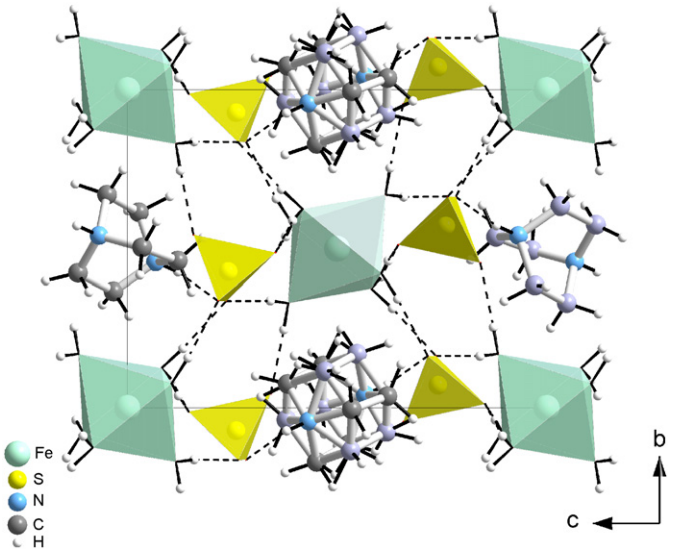

Fig. 1. Projection of the crystal structure of $(C_6H_{14}N_2)[Fe(H_2O)_6](SO_4)_2$ at room temperature. H bonds are shown as dashed lines (as in the following figures). The minor part of the disordered ($dabcoH_2$) group is in purple.

in the Ni [3] and Cu [4]-related phases, deviate somewhat from those in the literature [29]. This deviation seems to be a consequence of the disorder of the carbon atoms.

The $[Fe(H_2O)_6]^{2+}$ cations occupy the corners and the center of the unit cell while the $(dabcoH_2)^{2+}$ cations are located on the positions of the metal translated by $\frac{1}{2}$ along the *c* axis: they are then placed in the middle of the edges parallel to [0 0 1] and the center of the faces defined in the (ab) plane. Thus, the organic and inorganic cations alternate along the [0 0 1] and [1 1 0] directions and form mixed cationic layers perpendicular to the crystallographic *c* axis.

The asymmetric unit of the HT-phase contains only one independent regular SO_4 tetrahedron. The sulfate groups are stacked in a manner that they form anionic layers parallel to the cationic ones. The crystal structure is then described as an alternation of cationic and anionic layers along [0 0 1] (Fig. 1). In the present compound, the SO_4^{2-} ions play an important role in the cohesion of the crystal structure by linking the organic and inorganic cations via N–H…O and OW–H…O hydrogen bonds. Indeed, all the O atoms of the sulfate anion participate as acceptors in hydrogen bonds, i.e., from two H atoms bonded to N atoms and all water H atoms. Then, O2 and O3 are involved in two hydrogen bonds accepting two H atoms from water molecules, O4 accepts one dabcodiium H atom and one water H atom and O1 participates in only one hydrogen bond with water molecule. Within the intermolecular bonds, the donor–acceptor distances are composed between 2.697(3) and 2.796(3) Å with a mean distance D…O = 2.729 Å.

Although the crystal structure of $(C_6H_{14}N_2)[Fe(H_2O)_6](SO_4)_2$ is isomorphous to those of the nickel [3] and copper [4] compounds, significant differences are observed both in the direction of the charged-layers alternation and in the hydrogen bonds established between metal octahedra and sulfate tetrahedra. Indeed, the alternation of anionic and cationic layers is observed along [0 1 0] in the Ni and Cu phases and along [0 0 1] in the case of the title compound.

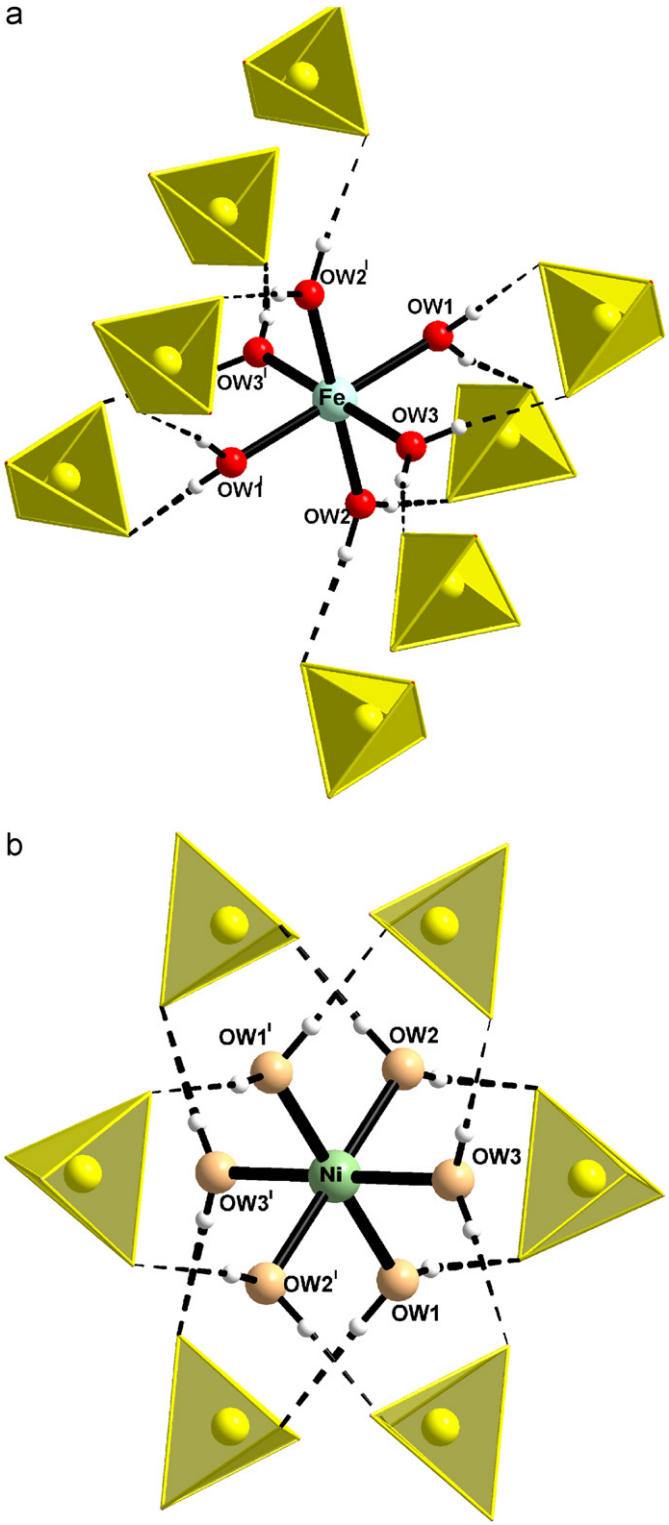

Fig. 2. Neighboring sulfates in the environment of $[M^{II}(H_2O)_6]^{2+}$ in (a) $(C_6H_{14}N_2)[Fe(H_2O)_6](SO_4)_2$ and (b) $(C_6H_{14}N_2)[Ni(H_2O)_6](SO_4)_2$ at room temperature.

Each Fe octahedron is surrounded by four sulfate groups H-bonded in a bidentate manner and four sulfate groups H-bonded in a monodentate fashion. This environment differs from that found in the Ni and Cu analogous compounds, in which the metal octahedron is surrounded by six sulfate tetrahedra only, connected via H bonds in a bidentate fashion. Figs. 2a and b show the neighboring sulfates in the environment of $[M^{II}(H_2O)_6]$ octahedron in $(C_6H_{14}N_2)[Fe(H_2O)_6](SO_4)_2$ and, for comparison, in the Ni-related phase [3].

3.1.2. Low-temperature structure (at −173 °C)

According to the X-ray diffraction study performed on a single crystal of $(C_6H_{14}N_2)[Fe(H_2O)_6](SO_4)_2$ at −173 °C, it can be concluded that the title compound undergoes a structural phase transition upon cooling. Indeed, the HT-phase (centrosymmetric space group $P2_1/n$, $Z=2$) transforms into a non-centrosymmetric structure variety, which crystallizes with the monoclinic symmetry, space group Cc, $Z=16$. Despite these important modifications in the structure packing and the symmetry, the LT-phase exhibits numerous similarities with the HT-phase, in particular through the alternation between the anionic and the cationic layers along the c axis. The supramolecular character of the phase is preserved. Indeed, the crystal structure of $(C_6H_{14}N_2)[Fe(H_2O)_6](SO_4)_2$ at −173 °C is built from $[Fe(H_2O)_6]^{2+}$, $(SO_4)^{2-}$ and fully ordered $(C_6H_{14}N_2)^{2+}$ ions linked together by an extensive three-dimensional H-bonding network. Fig. 3 shows a projection of the structure viewed down the crystallographic a axis.

The asymmetric unit of the LT-phase contains four independent iron atoms. As in the HT-phase structure the octahedra around the Fe^{2+} cations are slightly distorted (see OW–Fe distances and OW–Fe–OW angles in Table 1). These irregular octahedra are separated with a shortest Fe–Fe distance equal to 7.897 Å, which is shorter than that

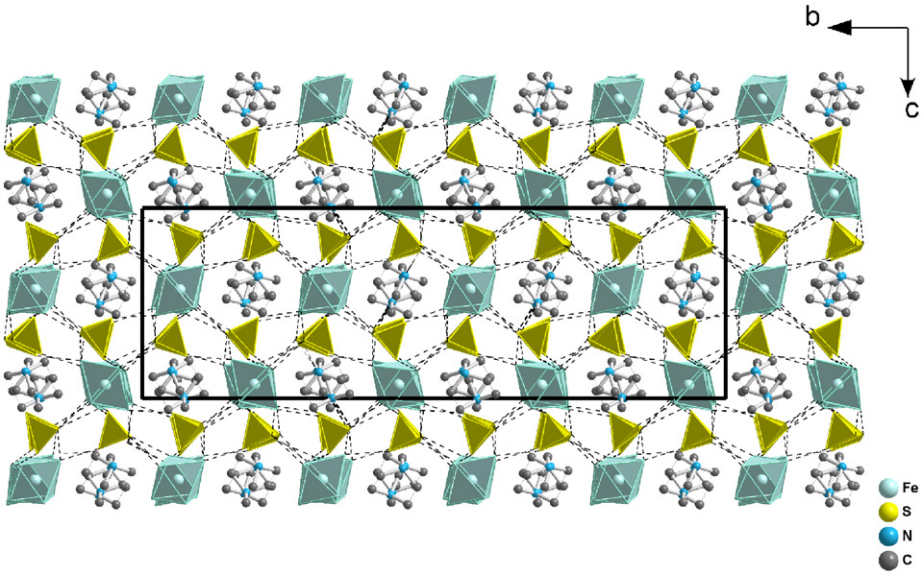

Fig. 3. Projection of the structure of $(C_6H_{14}N_2)[Fe(H_2O)_6](SO_4)_2$ at −173 °C along the a-axis. H atoms are omitted for clarity.

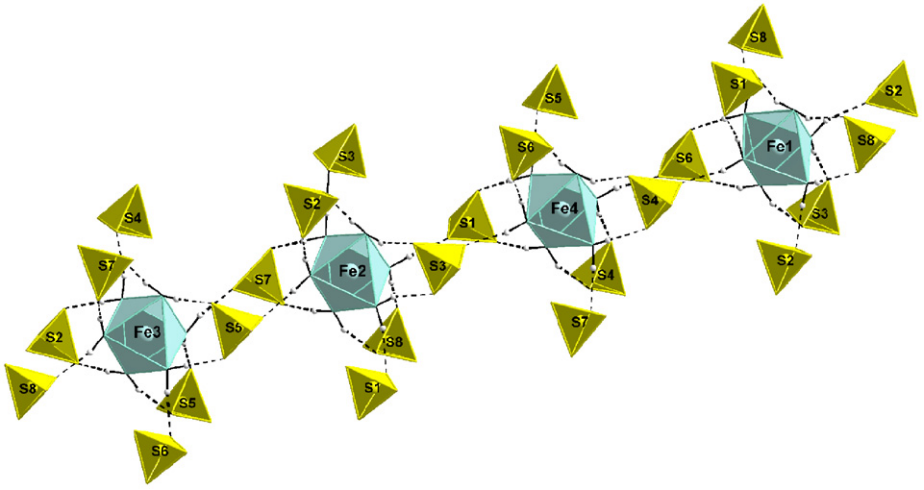

Fig. 4. Part of the structure of $(C_6H_{14}N_2)[Fe(H_2O)_6](SO_4)_2$ at −173 °C, showing the neighboring sulfate tetrahedra around each Fe(II) octahedron.

found in the room temperature structure (7.964 Å). This result is a consequence of the dabcodiium cations ordering, as shown previously in the Ni- and Cu-related compounds [3,4]. On the other hand, this intermetallic distance is longer than that found in the analogous compound containing piperazine as template, Fe–Fe = 7.839 Å [2]. This difference in the metal–metal distance between the two phases certainly depends on the size and the shape of the amino group involved in the structures, i.e. $(C_6H_{14}N_2)^{2+}$ and $(C_4H_{12}N_2)^{2+}$. The iron polyhedra are linked together by OW–H…O hydrogen bonds through the sulfate tetrahedra. Fig. 4 shows that each metallic octahedron is connected to four SO_4^{2-} anions in a bidentate manner and four sulfate groups in a monodentate fashion, as seen in the HT-phase.

The organic ions become fully ordered at −173 °C and present geometrical characteristics (C–N distances and C–N–C angles) usually found in analogue compounds containing dabco as template [3–5,30]. They stack in columns parallel to the three axes to generate, together with the Fe octahedra which present the same feature, mixed organic–inorganic cationic layers parallel to [0 0 1] (Fig. 3). The two types of cations alternate along [1 0 2]. According to Fig. 5, the structure of the LT-phase can also be described as an alternation between organic and inorganic layers along the *a* axis.

In the present structure, the asymmetric unit contains eight independent sulfur atoms located on general positions and tetrahedrally coordinated by four oxygen atoms. These anions link the organic and inorganic cations by two types of hydrogen bonds: OW–H…O and N–H…O. Within the intermolecular bonds, the N…O distances vary between 2.648(7) and 2.722(7) Å (mean value of 2.683(7) Å) and the OW…O distances range from 2.687(6) to 2.859(7) Å (mean value of 2.734(6) Å). These values are not significantly different from those found at room temperature. It can be concluded that the hydrogen bond network is not considerably affected by the ordering of the organic moiety, although a more rigid structure was expected at low temperature.

A careful examination of the positions of the different entities in this structure shows that anions and cations stack along [1 1 2] and [3 0 2] in a *ABACABAC*…fashion, where A:SO_4;B:[$Fe(H_2O)_6$] and C:($C_6H_{14}N_2$), and are held together by N–H…O and OW–H…O hydrogen bonds. Figs. 6a and b present projections of the crystal structure of $(C_6H_{14}N_2)[Fe(H_2O)_6](SO_4)_2$ at −173 °C showing this feature.

3.2. Phase-transition characterization

3.2.1. Differential-scanning calorimetry

In order to detect the expected phase transition at low temperature, a differential-scanning calorimetry (DSC) measurement was carried out from −50 to 50 °C. Fig. 7 shows the appearance of only one phase transition at about −2.3 °C. The characteristic dynamical values of this phase transition are:

Increasing temperature	Decreasing temperature
T_o (onset) = −4.1 ± 0.3 °C	T_o (onset) = 4 ± 0.3 °C
T_s (peak) = −2.3 ± 0.3 °C	T_s (peak) = −1.4 ± 0.3 °C
$\Delta H = 541.7\ J\ mol^{-1}$	$\Delta H = -654.3\ J\ mol^{-1}$
$\Delta S = 2.001\ J\ mol^{-1}\ deg^{-1}$	$\Delta S = 2.411\ J\ mol^{-1}\ deg^{-1}$

The shape of the heat anomaly and the crystallographic studies determined at 20 and −173 °C suggest the reversibility of the phase transition classified of the first order and clearly indicates its discontinuous nature.

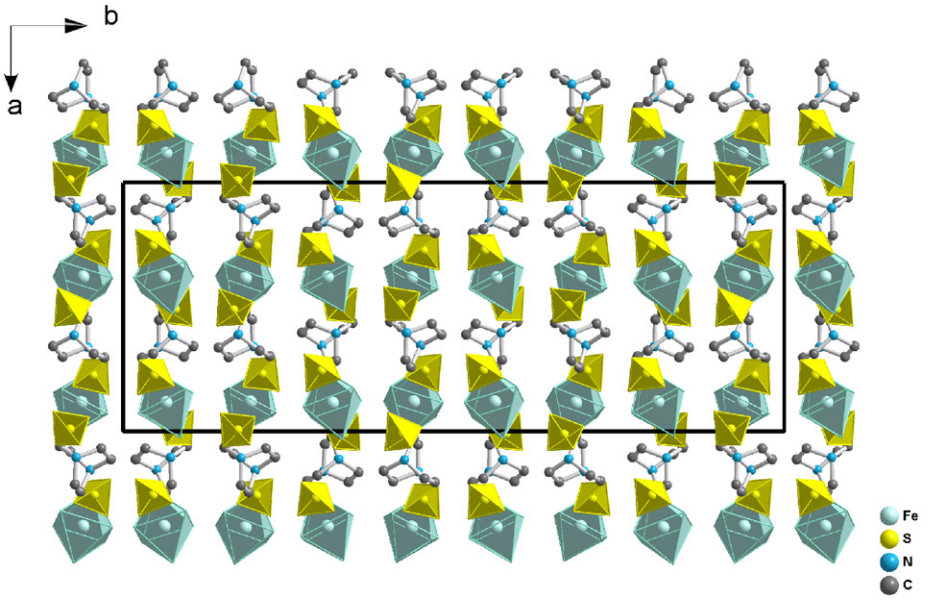

Fig. 5. Projection of the structure of $(C_6H_{14}N_2)[Fe(H_2O)_6](SO_4)_2$ at −173 °C along the *c*-axis.

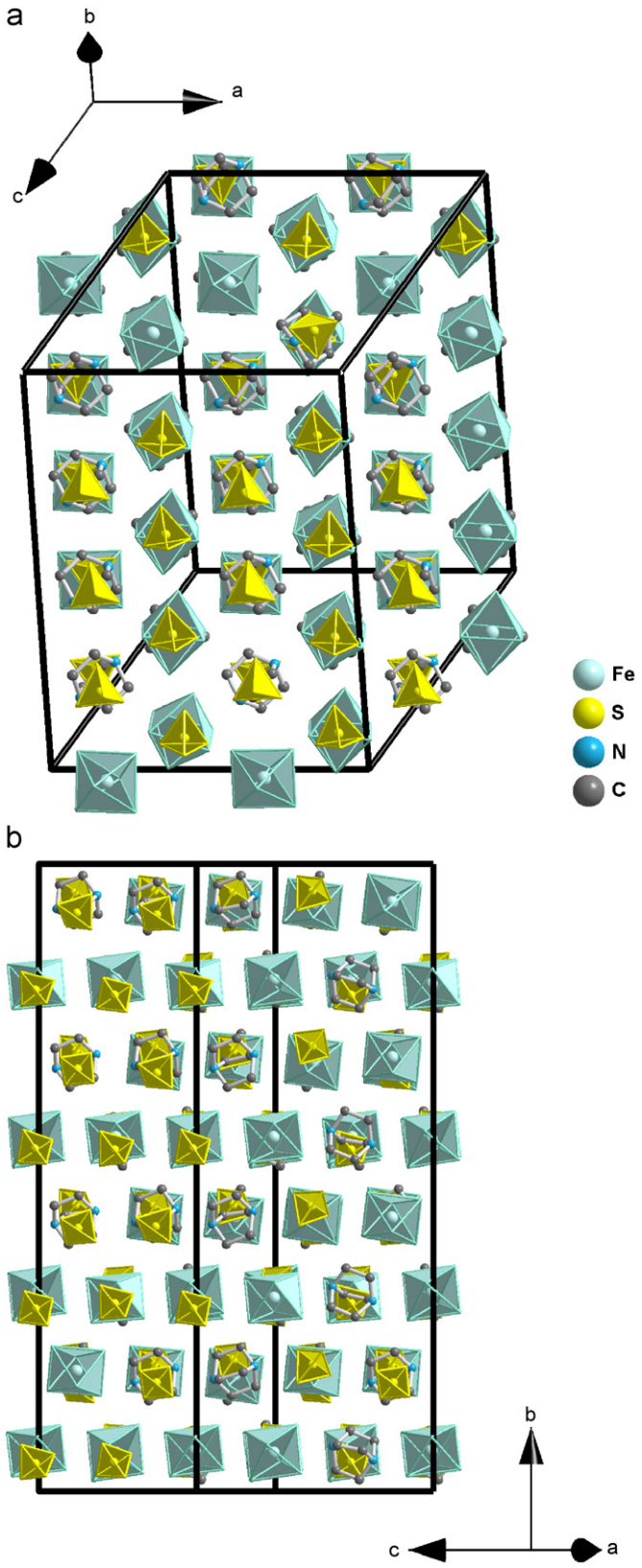

Fig. 6. Projection of the structure of $(C_6H_{14}N_2)[Fe(H_2O)_6](SO_4)_2$ at −173 °C along (a) [1 1 2] and (b) [3 0 2], showing the alternation between anions and cations along these two directions.

3.2.2. Dielectric properties

The electrical data measured as an impedance Z^* have been converted into permittivity ε^* using the relation, $\varepsilon^* = 1/iwC_0Z^*$, where C_0 is the vacuum capacitance [31]. Fig. 8 shows the temperature dependence of the real part of the complex permittivity, ε', at six frequencies: 100 Hz, 1, 10, 100 and 465 KHz and 1 MHz. The phase transition detected by DSC is confirmed by the dielectric study. Indeed, only one dielectric anomaly is observed as reported in Fig. 7. This diffuse peak is significantly stronger than that found in the copper related compound [4] to reach the amplitude of 330 units at 100 Hz. It is interesting to note that increasing the frequency leads to increasing the phase-transition temperature from −3 °C at 100 Hz to 22 °C at 100 kHz. Furthermore, no hysteresis was detected from spontaneous polarization measurements upon cooling from room temperature to −5 °C, i.e., in the region where dielectric permittivity is non-null. All these results suggest that the studied system presents the main characteristics of

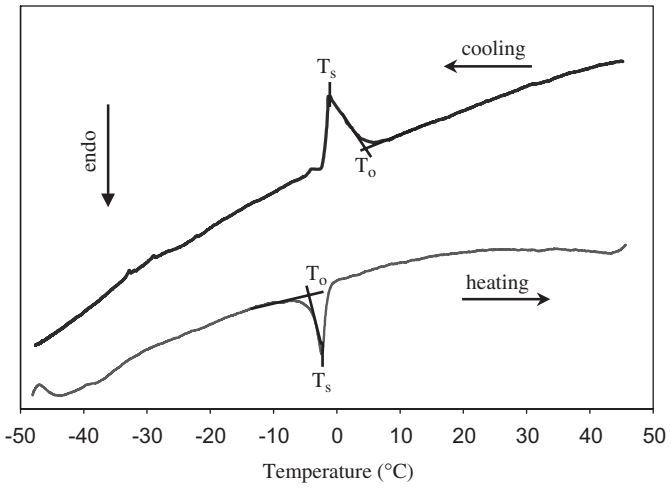

Fig. 7. DSC curve obtained by cooling and heating $(C_6H_{14}N_2)[Fe(H_2O)_6](SO_4)_2$ from −50 to 50 °C.

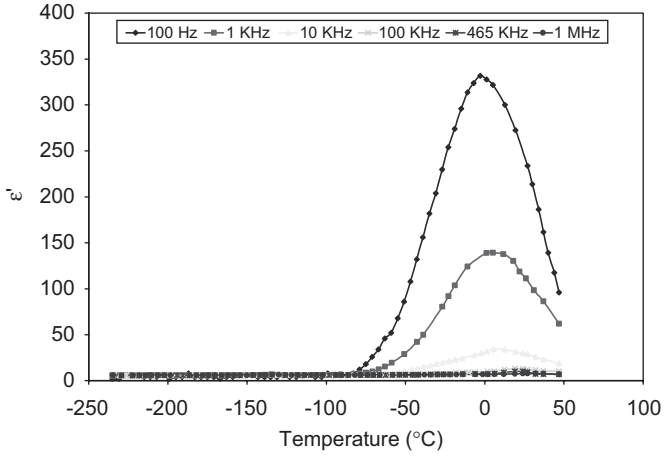

Fig. 8. Temperature dependence of ε′ at different frequencies.

relaxor ferroelectrics. Within this class of materials, the occurrence of the dielectric response over such a larger temperature range than the DSC transition is usually connected with the state of disorder of the HT-phase. Here, it is consistent with the ordering of the dabcodiium cations upon cooling, which thus appears quite slow. This broad dielectric permittivity peak is similar to that found in the copper-related phase [4], in $(C_5H_{10}NH_2)SbCl_6 \cdot (C_5H_{10}NH_2)Cl$ [32] and in common relaxor ferroelectrics such as barium titanates [33].

3.2.3. Polarized microscope observations

In order to point out a possible ferroelastic behavior of the crystal at low temperature, microscopic observations were made, using Leitz optical polarization microscope (ortholux2-pol type), at several temperatures below and above the transition point. This experiment excludes any para-ferroelastic nature of the transition. Indeed, photographs given in Fig. 9 did not show any ferroelastic domain structure over the wide temperature range, in agreement with a disorder–order transition.

3.3. Thermal decomposition

The thermal decomposition of $(C_6H_{14}N_2)[Fe(H_2O)_6](SO_4)_2$, studied by temperature-dependent X-ray diffraction (TDXD) and thermogravimetry (TG) under flowing air, proceeds through three main stages. The first step corresponds to the full dehydration of the precursor, the second stage coincides with the decomposition of the organic moiety, together with the partial release of sulfate groups, and the third stage is characterized by the removal of remaining sulfates to form the final iron oxide.

Fig. 10 shows the successive powder patterns obtained during the thermal decomposition of the title compound upon heating. The TG curve for $(C_6H_{14}N_2)[Fe(H_2O)_6](SO_4)_2$ is displayed in Fig. 11. It is shown that the first transformation occurs in the temperature range 80–133 °C. The weight loss of 22.54% is in agreement with the departure of six water molecules (calculated weight loss, 22.96%), thus leading to the anhydrous phase $(C_6H_{14}N_2)Fe(SO_4)_2$ amorphous to X-rays (Fig. 10). The decomposition of the anhydrous phase starts at about

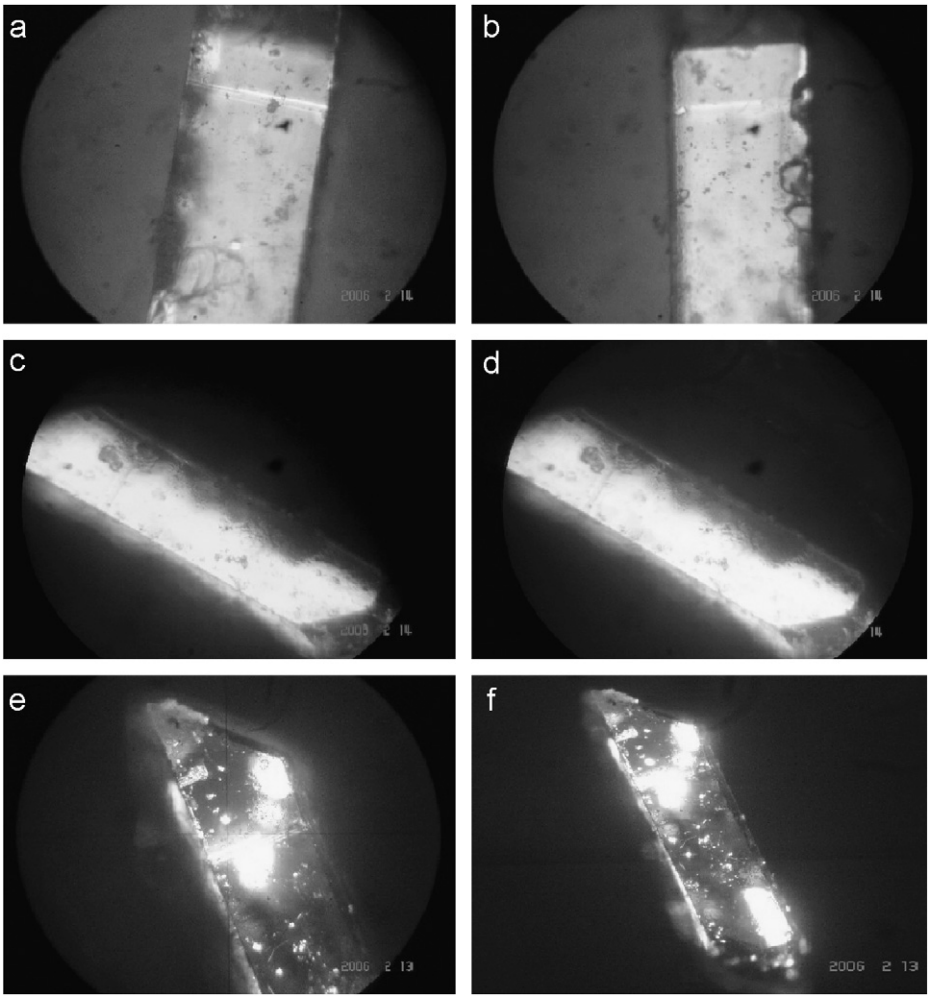

Fig. 9. Photographs of $(C_6H_{14}N_2)[Fe(H_2O)_6](SO_4)_2$ crystal upon heating: (a) 128 K; (b) 202 K; (c) 216 K, (d) 253 K, (e) 273 K and (f) 280 K.

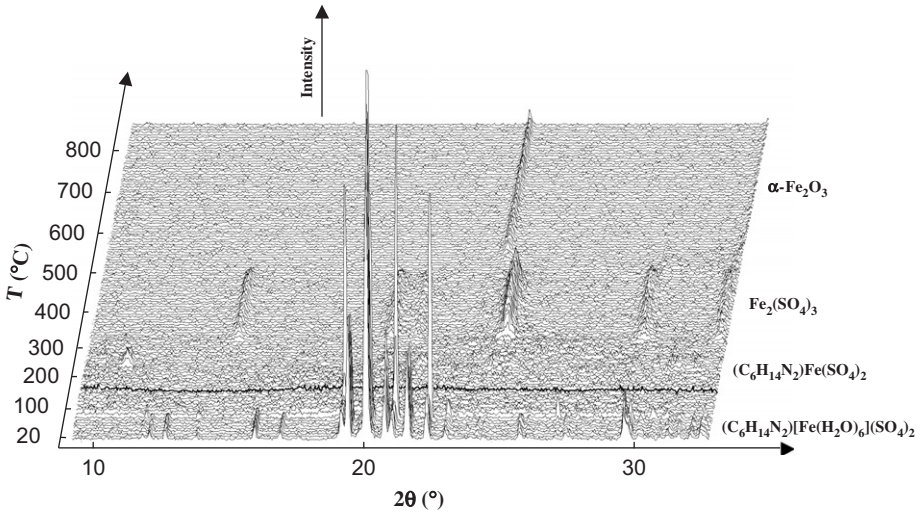

Fig. 10. TDXD plot for the decomposition of $(C_6H_{14}N_2)[Fe(H_2O)_6](SO_4)_2$ in air.

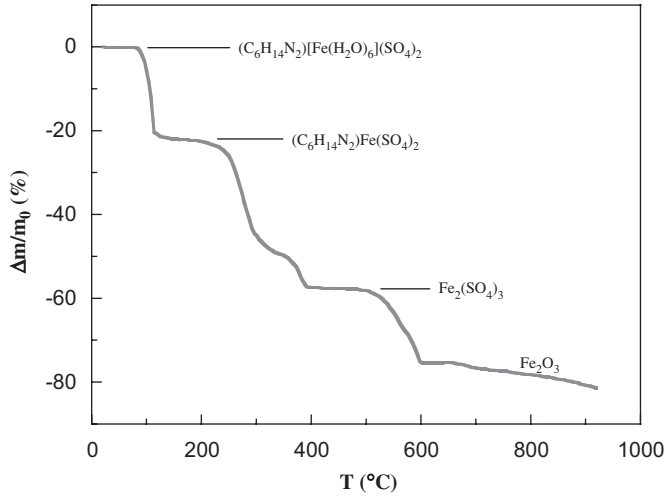

Fig. 11. TG curve for the decomposition of $(C_6H_{14}N_2)[Fe(H_2O)_6](SO_4)_2$ in flowing air (15 °C h^{-1}).

190 °C on the TG curve and leads to a crystalline compound clearly observed between 360 and 510 °C on the TDXD plot. Interrogation of the ICDD powder diffraction file [34] revealed that this phase is iron sulfate $Fe_2(SO_4)_3$ (PDF N° 01-073-0148). This transformation takes place with an observed weight loss of 57.45% (calculated weight loss, 57.50%). The final stage corresponds to the decomposition of the iron sulfate into α-Fe_2O_3 (PDF N° 01-088-2359).

4. Conclusions

The above results indicate that the new dabcodiium hexaaquairon(II) bis(sulfate), $(C_6H_{14}N_2)[Fe(H_2O)_6](SO_4)_2$, synthesized by slow evaporation, undergoes a structural phase transition at low temperature. The crystallographic studies show that it crystallizes in the centrosymmetric space group $P2_1/n$ at room temperature. Its crystal structure is built from isolated ions: $[Fe(H_2O)_6]^{2+}$, $(SO_4)_2^{2-}$ and disordered $(C_6H_{14}N_2)^{2+}$ linked together by hydrogen bonds only. The DSC experiment reveals that it undergoes a first-order phase transition at −2.3 °C accompanied by strong modifications of the space group and the unit cell parameters. The X-ray examination of this hybrid material at −173 °C demonstrates that it crystallizes in the non-centrosymmetric space group *Cc* and that the organic cations become fully ordered. The phase transition has been characterized by dielectric study and optical observations. The ferroelastic nature has been excluded according to polarized microscope observations, but the behavior of the dielectric permittivity suggests a possible relaxor–ferroelectric behavior associated with a disorder–order transition. The thermal decomposition of the title compound proceeds through three stages: the departure of the six water molecules giving rise to anhydrous phase amorphous to X-rays, then the decomposition of this anhydrous compound to form the iron(III) sulfate and finally the removal of remaining sulfates to form the final iron oxide.

This study offers a promising route to elaborate new dielectric sulfate materials, such as long-established low-temperature ferroelectric trivalent metal sulfates [18]. Indeed, guanidine and alkylamine may be replaced by other amine groups, and Al^{3+} or Ga^{3+} by transition metals, that allow many possibilities of obtaining supramolecular sulfates. In addition, the transition temperature of the former sulfates are about 170 K, while for the title compound, $(C_6H_{14}N_2)[Fe(H_2O)_6](SO_4)_2$, the transition is observed at ca. 270 K. A phase transition in the vicinity of the ambient allow thinking of new switching dielectrics.

The authors express their sincere thanks to Dr. T. Roisnel (Centre de Diffractométrie X, Université de Rennes I) and G. Marsolier for their respective assistance in single-crystal and powder X-ray diffraction data collection, Dr R. Von der Mühll (ICMCB-CNRS Université Bordeaux 1) for the optical observations and Pr D.

Lemoine (Laboratoire Foton, INSA de Rennes) for spontaneous polarization measurements.

Appendix A. Supplementary materials

The online version of this article contains additional supplementary data. Please visit doi:10.1016/j.jssc.2007.10.019

References

[1] W. Rekik, H. Naïli, T. Mhiri, T. Bataille, Acta Crystallogr. E 61 (2005) m629–m631.
[2] W. Rekik, H. Naïli, T. Bataille, T. Roisnel, T. Mhiri, Inorg. Chim. Acta 359 (2006) 3954–3962.
[3] W. Rekik, H. Naïli, T. Bataille, T. Mhiri, J. Organomet. Chem. 691 (2006) 4725–4732.
[4] H. Naïli, W. Rekik, T. Bataille, T. Mhiri, Polyhedron 25 (2006) 3543–3554.
[5] W. Rekik, H. Naïli, T. Mhiri, T. Bataille, J. Chem. Crystallogr. 37 (2006) 147–155.
[6] Y. Xing, Y. Liu, Z. Shi, H. Meng, W. Pang, J. Solid State Chem. 174 (2003) 381–385.
[7] T. Bataille, D. Louër, J. Solid State Chem. 177 (2004) 1235–1243.
[8] T. Bataille, D. Louër, J. Mater. Chem. 12 (2002) 3487–3493.
[9] C. Ruiz-Valero, C. Cascales, B. Gomez-Lor, E. Gutierrez-Puebla, M. Iglesias, M. Angeles Monge, N. Snejko, J. Mater. Chem. 12 (2002) 3073–3077.
[10] A. Norquist, M.B. Doran, P.M. Thomas, D. O'Hare, Dalton Trans. (2003) 1168–1175.
[11] Y. Xing, Z. Shi, G.H. Li, W.Q. Pang, Dalton Trans. (2003) 940–943.
[12] C.N. Morimoto, E.C. Lingafelter, Acta Crystallogr. B 26 (1970) 335–341.
[13] M. Doran, A.J. Norquist, D. O'Hare, Chem. Commun. (2002) 2946–2947.
[14] M. Dan, J.N. Behera, C.N.R. Rao, J. Mater. Chem. 14 (2004) 1257–1265.
[15] L.F. Kirpichnikova, E.F. Andreev, N.R. Ivanov, L.A. Shulakov, V.M. Varikash, Kristallografiya 33 (1988) 1437–1440.
[16] A.N. Holden, B.T. Matthias, W.J. Merz, J.P. Remeika, Phys. Rev. 98 (1955) 546.
[17] N. Galesic, V.B. Jordanovska, Acta Crystallogr. C 48 (1992) 256–258.
[18] L.F. Kirpichnikova, L.A. Shuvalov, N.R. Ivanov, B.N. Prasolov, E.F. Andreyev, Ferroelectrics 96 (1989) 313–317.
[19] A. Pietraszko, K. Lukaszewicz, L.F. Kirpichnikova, Polish J. Chem. 67 (1993) 1877–1884.
[20] N.W. Grimes, H.F. Kay, M.W. Webb, Acta Crystallogr. 16 (1963) 823–829.
[21] E.N. Maslen, S.C. Ridout, K.J. Watson, F.H. Moore, Acta Crystallogr. C 44 (1988) 409–412.
[22] J.-X. Pan, G.-Y. Yang, Y.-Q. Sun, Acta Crystallogr. E 59 (2003) m286–m288.
[23] Nonius, Kappa CCD Program Software, Nonius BV, Delft, The Netherlands, 1998.
[24] Z. Otwinowski, W. Minor, C.W. Carter, R.M. Sweet, in: Methods in Enzymology, 276, Academic Press, New York, 1997, p. 307.
[25] J. de Meulenaer, H. Tompa, Acta Crystallogr. 19 (1965) 1014–1018.
[26] S. Parkin, B. Moezzi, H. Hope, J. Appl. Crystallogr. 28 (1995) 53–56.
[27] G.M. Sheldrick, SHELXS-97, Programs for Crystal Structure Solution, University of Göttingen, Germany, 1997.
[28] G.M. Sheldrick, SHELXL-97, Programs for Crystal Structure Refinement, University of Göttingen, Germany, 1997.
[29] K. Jayaraman, A. Choudhury, C.N.R. Rao, Solid State Sci. 4 (2002) 413–422.
[30] Y.-J. Zhao, X.-H. Li, S. Wang, Acta Crystallogr. E 61 (2005) m671–m672.
[31] T.M. Shchegoleva, L.D. Iskhakova, S.M. Ovanesyan, A.A. Shakhnazaryan, V.K. Trunov, Zh. Neorg. Khim. 28 (1983) 2271–2276.
[32] B. Bednarska-Bolek, A. Pietraszko, R. Jakubas, G. Bator, B. Kosturek, J. Phys.: Condens. Matter 12 (2000) 1143–1159.
[33] W. Xiaoyong, F. Yujun, Y. Xi, Appl. Phys. Lett. 83 (2003) 2031–2033.
[34] International Centre for diffraction data, Powder Diffraction File, Newtown Square; PA, 2002.